metals

MDPI

Article

Enhanced Adsorption Removal of Pb(II) and Cr(III) by Using Nickel Ferrite-Reduced Graphene Oxide Nanocomposite †

Lakshmi Prasanna Lingamdinne [1], Im-Soon Kim [1], Jeong-Hyub Ha [2], Yoon-Young Chang [1], Janardhan Reddy Koduru [1,*] and Jae-Kyu Yang [3,*]

1 Department of Environmental Engineering, Kwangwoon University, Seoul 01897, Korea; swethasiri86@gmail.com (L.P.L.); imsoon99@hanmail.net (I.-S.K.); yychang@kw.ac.kr (Y.-Y.C.)
2 Department of Integrated Environmental Systems, Pyeongtaek University, Gyeonggi-Do 17869, Korea; jhha@ptu.ac.kr
3 Ingenium College of Liberal Arts, Kwangwoon University, Seoul 01897, Korea
* Correspondence: reddyjchem@gmail.com (J.R.K.); jkyang@kw.ac.kr (J.-K.Y.); Tel.: +82-(02)-940-5496 (J.R.K.); +82-(02)-940-5769 (J.-K.Y.); Fax: +82-(02)-918-5774 (J.R.K.); +82-(02)-917-5769 (J.-K.Y.)
† Electronic Supplementary Materials (ESM) available.

Received: 12 April 2017; Accepted: 13 June 2017; Published: 19 June 2017

Abstract: The heavy metals, such as Pb(II) and radioisotope Cr(III), in aqueous solutions are toxic even at trace levels and have caused adverse health impacts on human beings. Hence the removal of these heavy metals from the aqueous environment is of the utmost importance to protect biodiversity, hydrosphere ecosystems, and human beings. In this study, the reduced graphene oxide based inverse spinel nickel ferrite (rGONF) nanocomposite has been prepared and was utilized for the removal of Pb(II) and Cr(III) from aqueous solutions. The prepared rGONF has been confirmed by X-ray photoelectron (XPS) and Raman spectroscopy. The surface characteristics of rGONF were measured by scanning electron microscopy (SEM), High-Resolution Transmission Electron Microscope (HR-TEM), and Brunauer-Emmett-Teller (BET) surface analysis. The average particle size of rGONF was found to be 32.0 ± 2.0 nm. The surface site density for the specific surface area (Ns) of rGONF was found to be 0.00238 mol·g^{-1}, which was higher than that of the graphene oxide (GO) and $NiFe_2O_4$, which was expected. The prepared rGONF has been successfully applied for the removal of Pb(II) and Cr(III) by batch mode. The batch adsorption studies concluded that the adsorption of Pb(II) and Cr(III) onto rGONF was rapid and the adsorption percentage was more than 99% for both metal ions. The adsorption isotherm results found that the adsorptive removal of both metal ions onto rGONF occurred through monolayer adsorption on a homogeneous surface of rGONF. The pH-edge adsorption results suggest the adsorption occurs through an inner-sphere surface complex, which is proved by 2-pKa-diffusion model fitting, where the pH-edge adsorption data was well fitted. The adsorption of metal ions increased with increasing temperature. The overall obtained results demonstrated that the rGONF was an effective adsorbent for Pb(II) and Cr(III) removal from wastewater.

Keywords: adsorption; heavy metals; reduced graphene oxide; nickel ferrite; magnetic materials; nanocomposites

1. Introduction

Nowadays, graphene and graphene oxide (GO) materials are widely used in many applications. However, due to the presence of decorated hydroxyl, carboxyl, and epoxy functional groups on the basal plane and plane edge [1], GO is more easily dispersed than graphene. Additionally, the durable

hydrophilicity of GO guarantees that it is a good candidate for many applications including drug delivery, harmful cell treatment, and water purification [2,3].

To enrich its functionalities, GO is always used as a host in various nanomaterials due to its large surface area and high reactivity [4,5]. The incorporation of inorganic nanoparticles (NPs) into GO well improved its performance in various applications. Moreover, GO is a good candidate for constructing GO-based metal oxide composites. In addition, GO-based metal oxide materials possess a good ability to adsorb heavy metal ions and organic pollutants [4,5]. However, the limitations in separation and the following recycling process have significantly restricted their applications. However, the introduction of magnetic NPs onto GO can improve its efficient adsorption behavior as well as overcome separation and recycling problems. Previous reports have proved that the magnetic NPs/GO composites have an amazing removal response for pollutants, including chromium [4–6], copper [7,8], arsenic [9–11], cadmium [12], lead [13], cobalt [14], and organic dyes [14–16]. Nickel ferrite-GO composites have been studied as a promising reaction media because the Ni^{2+} in the nickel ferrites shows unique properties such as high catalytic efficiency with high charge (electron) transfer capacity compared to the iron ferrites [17,18]. Moreover, in our previous studies, GO-based nickel ferrite has been used for the removal of U(VI), Th(IV) [19], and anionic contaminants As(III)/As(V) (oxoacids) [10]. However, the reduction of the GO-based nickel ferrite composite may increase its surface area with enhanced adsorption capacity. In addition, the reduced graphene oxide based inverse spinel nickel ferrite (GONF) has not yet been used for adsorptive removal of cationic heavy metals, to the best of our knowledge. Hence, in the present study, the cationic type heavy metals (Cr(III) and Pb(II)) adsorption mechanism (which is different with anionic type heavy metals) onto the reduced GO-based nickel ferrite composite was evaluated. The removal of these heavy metals from the aqueous environment is of the utmost importance to protect biodiversity, hydrosphere ecosystems, and human beings. The adsorption capacity of the prepared rGONF for Pb(II) and radioactive isotope Cr(III) were comparable with the other reported adsorbents (Table 1). In addition, rGONF can be easily separated by an external magnetic field without the loss of any structural changes and can be reused up to four cycles. Hence, the synthesized rGONF could be justified as an efficient adsorbent and reasonable for the treatment of heavy metals.

Table 1. Comparison of the adsorption capacities of reduced graphene oxide based nickel ferrite (rGONF) with the other reported adsorbents for Pb(II) and Cr(III). graphene oxide (GO):

Adsorbent	Metal Ion Removal, $mg \cdot g^{-1}$	
	Pb(II)	**Cr(III)**
Magnetic-GO [8]	6	-
Coal fly ash [20]	45.25	22.94
Diatomaceous earth clay (DAT) [21]	19.608	14.225
DAT-Hexadecyltrimethylammonium Bromide [21]	24.271	22.779
GO [22]	-	92.65
Lonicera japonica flower powder [23]	19.61	-
Porous $NiFe_2O_4$ [24]	48.98	-
Celtek clay [25]	18.08	21.55
rGONF [This Work]	121.95	126.58
GO [This Work]	44.56	36.45
Nickel Ferrite ($NiFe_2O_4$) [This Work]	25.78	20.58

2. Materials and Methods

2.1. Materials

$Pb(NO_3)_2$ and $Cr(NO_3)_3 \cdot 9H_2O$, supplied by Samchun Pure Chemicals Co., Ltd. (Pyeongtaek, Korea), were used for the preparation of the metal ions, Pb(II) and Cr(III), stock solution (1000 $mg \cdot L^{-1}$). The reagents $Fe(NO_3)_3 \cdot 9H_2O$, $Ni(NO_3)_3 \cdot 9H_2O$, HCl (40%), and NH_4OH (56.6%) used for the

preparation of rGONF, were obtained from Samchun Pure Chemicals Co. Ltd. (Pyeongtaek, Korea). The hydrazine hydrate supplied by Sigma-Aldrich (St. Louis, MO, USA) was used for the reduction of GO. All chemicals were of analytical reagent grade and were used as supplied.

2.2. Preparation Method of rGONF

rGONF was prepared by the procedure reported in our previous paper [19]. Briefly described here, hydrazine hydrate (10 mL) was slowly added to the solution containing 0.5 g GO (GO prepared by using the well-known Hummer's method from Graphite flakes procured from Sigma-Aldrich, St. Louis, MO, USA) and a 2:1 molar ratio of Fe^{3+}:Ni^{2+} at pH $\geq$ 12 in a nitrogen atmosphere for the preparation of rGONF. Then, the solution temperature was slowly raised to 120 °C with constant stirring for 5 h and resulted in a black precipitation in the solution. The solution was then cooled to room temperature and the resulting black precipitate was thoroughly washed with double distilled de-ionized water/ethanol. The resulting black rGONF was collected by magnetic separation, and then dried at 60 °C under vacuum for 12 h.

2.3. Adsorption Characteristic Studies of rGONF

Typical batch adsorption experiments were performed in a 50 mL polyethylene falcon tube (BD Falcon, Seoul, Korea) containing 0.4 g·L^{-1} of rGONF with 50 mL of the desired concentration of metal ions, Pb(II) (at pH 5.0) and Cr(III) (at pH 4.0). The pH of the solutions was adjusted with 0.1 mol·L^{-1} of HCl or NaOH and measured by using a 340i pH meter (WTW Measurement Systems INC, Dinslaken, Germany). The falcon tubes were shaken using a rotator shaker (Finemould Precision Ind. Co., Seoul, Korea) at room temperature for a pre-determined equilibrium time. The reagent blank (with metal ions without nanocomposites) was checked for measuring the adsorption caused by the falcon tube, which was negligible. The adsorbents were separated using an external magnetic field and the aqueous solution was filtered using a 0.45 μm membrane syringe filter (Advantec MFC, Inc., Tokyo, Japan) The residual concentrations of both heavy metals in the filtrate were measured by using an Optima 2100 DV inductive coupled plasma-optical emission spectroscopy (ICP–OES) (Perkin-Elmer, Waltham, MA, USA) equipped with an auto-sampler. The desorption of heavy metals from the loaded rGONF was carried out using a 1.0 mol·L^{-1} HNO_3 solution. All investigations were carried out in triplicate to avoid discrepancies in the experimental results and the values reported are mean ± standard deviation (SD). The linear fits were used for checking the suitability of the adsorption data.

The amount of Pb(II) and Cr(III) adsorbed onto rGONF was calculated from the mass balance between the initial (C_o) and equilibrium (C_e) concentrations (mg·L^{-1}) of metal ions. The metal ions uptake capacity at equilibrium t, was calculated by $q_e = (C_o - C_e) \times V/M$, where V is the volume of the aqueous solution (L) and M is the adsorbent mass (g). The adsorption percentage (% R_s) of metal ions was calculated by the following equation: $\%R_s = (\frac{C_0 - C_e}{C_0}) \times 100$. The batch adsorption experiments were studied under varying operating conditions, including pH (2.0–7.0), contact time (0–90 min), adsorbent dosage (0.1–0.8 g·L^{-1}), ionic strength (0.005–0.5 mol·L^{-1}), and temperature (298–328 ± 2 K) to understand the adsorption mechanism of the rGONF for heavy metal ions.

2.4. 2-pKa-Diffusion Layer Modeling (2-pKa-DLM) Fitting by Using the Visual Minteq-3.0 Software

The modelling software Visual Minteq-3.0 (USEPA's MINTEQA2 software, Athens, Georgia) was used to evaluate the diffuse layer model (DLM) fitting. It was used to quantify the surface charge effects on the adsorption trends and to determine the best fit for the surface complexation constants of Pb(II) and Cr(III) onto rGONF. For model prediction, the surface site density of rGONF was calculated using the potentiometric titration data along with the specific surface area of rGONF (167.26 $m^2 \cdot g^{-1}$). The calculated surface site concentration (Ns) of rGONF was found to be 0.00238 mol·g^{-1}.

2.5. Preparation of Real Ground Water Spiked with Pb(II) or Cr(III)

Real ground water was collected from Yullyang-dong, Sangdang-gu, Cheongju-Si, Republic of Korea and its physical and chemical compositions are reported in Table 2. 10 mL of the desired concentration of Pb(II) or Cr(III) was added to 1 L of real ground water for the preparation of the spiked real ground water samples. These samples were used for the adsorptive removal of both heavy metals by using 0.4 $g \cdot L^{-1}$ of rGONF at the established adsorption experimental conditions.

Table 2. Physical and chemical compositions of real water samples collected from Yullyang-dong, Sangdang-gu, and Cheongju-Si, Republic of Korea (N = 3, mean values reported here, the standard deviation is less than 5%).

Physical or Chemical Compositions	Value or Concentration
pH	6.72
Oxidation-Reduction Potential (ORP)	171.3 mV
Dissolved Oxigen (DO)	2.73 $mg \cdot L^{-1}$
Electrical Conductivity (EC)	0.265 $mS \cdot cm^{-1}$
Ca^{2+}	65.06 $mg \cdot L^{-1}$
Na^{+}	16.09 $mg \cdot L^{-1}$
K^{+}	1.16 $mg \cdot L^{-1}$
Mg^{2+}	7.68 $mg \cdot L^{-1}$
Cl^{-}	14.29 $mg \cdot L^{-1}$
NO_3^{-}	14.30 $mg \cdot L^{-1}$
SO_4^{2-}	21.10 $mg \cdot L^{-1}$
F^{-}	Not detected
HCO_3^{-}	166.4 $mg \cdot L^{-1}$
Pb^{2+} or Cr^{3+}	Not detected

3. Results and Discussion

3.1. Characterization of Prepared rGONF and the Adsorption Mechanism of Pb(II) and Cr(III) onto rGONF

3.1.1. Structural Characterization of Prepared rGONF

X-ray photoelectron spectroscopy (XPS) analysis of rGONF was performed using ESCALAB–210 (Thermo Fisher Scientific, Madrid, Spain) and the results are shown in Figure 1a. Figure 1a shows that the oxygen peak at around 532.4 eV indicates the presence of oxygen in GO, while the formation of rGONF shifted the oxygen peak to a lower range at around 530.3 eV. The high binding energy intensity of the O (1s), Fe (2p), and Ni (2p) peaks confirmed the formation of rGONF from GO. In addition, the peaks at around 711.00 eV (Fe 2p) and 855.00 eV (Ni 2p) (Figure 1a) indicate the formation of inverse spinel $NiFe_2O_4$ or the formation of rGONF from GO.

In Figure 1b, the Raman spectra (IFS 66/S, FRA106/S (BRUKER OPTICK GMBH, Ettlingen, Germany)) of rGONF displays two prominent peaks at 1358 and 1606 cm^{-1}, which correspond to the D band and G band, respectively. It is well known that the G band corresponds to the first-order scattering of the E2 g mode observed for sp^2 carbon atoms and the D band is associated with the vibrations of sp^3 carbon atoms in rGONF. The D and G bands moved to a lower range of Raman shifts at ~1303 and ~1591 cm^{-1} and is associated with the reduction of GO. The formation of rGONF was further confirmed by the measurement of the structural disorder from the intensity ratio of the D and G bands (I_D/I_G). The intensity ratio of the D and G bands for rGONF was 1.094, showing an enhanced value compared to that of GO (0.96) [19]. In addition, the obtained rGONF has considerable crystallinity. This result indicates the presence of localized sp^3 defects within the sp^2 carbon frame upon the reduction or interaction of GO with $NiFe_2O_4$.

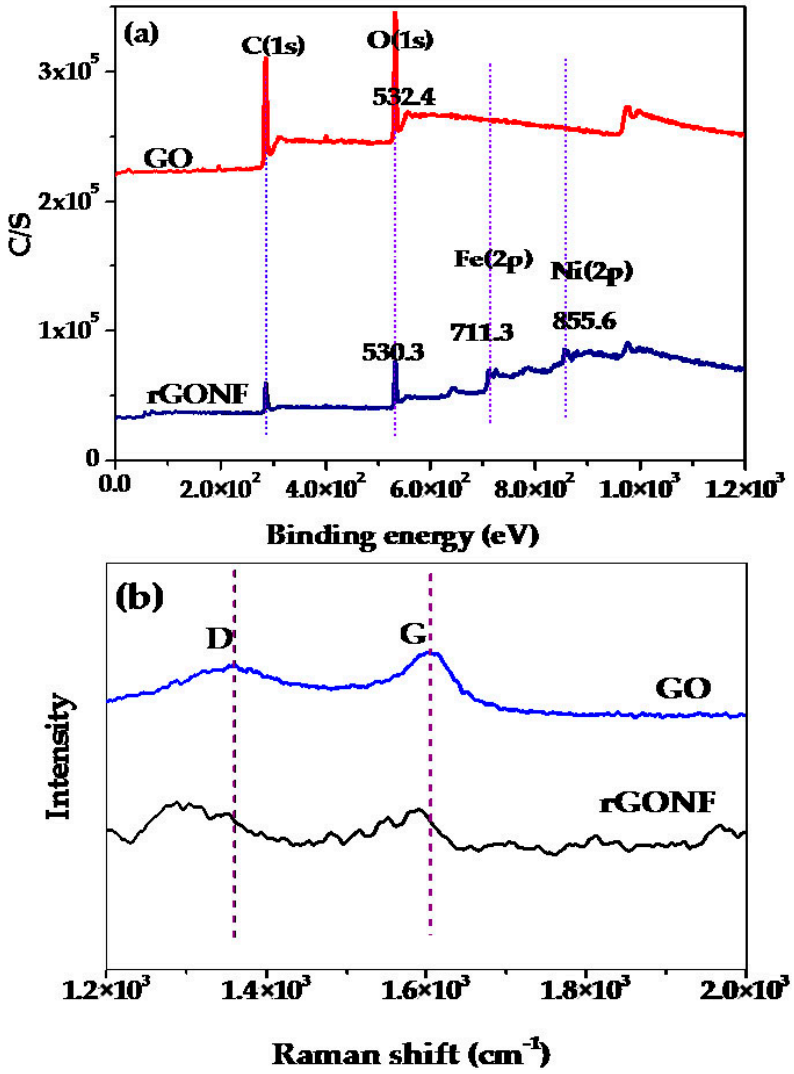

Figure 1. X-ray photoelectron spectroscopy (XPS) (**a**) and Raman spectral (**b**) analysis of rGONF. (Doted lines in the figure indicates the peaks comparison).

3.1.2. Surface Morphology and Size Characterization of Prepared rGONF

The surface characteristics of rGONF were studied by an Autosorb-1, (Quantachrome instruments, Boynton Beach, FL, USA) using Brunauer-Emmett-Teller (BET) surface analysis with nitrogen (N_2) adsorption-desorption isotherms. The BET surface area of rGONF is 167.26 $m^2 \cdot g^{-1}$ and the particle size is 34.46 nm. The modifications of GO (surface area: 12.04 $m^2 \cdot g^{-1}$) with nickel ferrite (surface area: 80 $m^2 \cdot g^{-1}$) increases its surface area to a large size and is favorable for enhancing its adsorption capacity. The resultant average pore volume and pore diameter of rGONF indicates the presence of nano-crystalline meso-porous composite particles. The resultant average particle sizes, 34.46 nm for rGONF, closely agree with the results obtained from the TEM studies (Figure 2) (which is measured by a High-Resolution Transmission Electron Microscope (HR-TEM) (JEM-4010, JEOL, Peabody, MA, USA)). Based on these overall results, the average particle size of rGONF was found to be 32.0 $\pm$ 2.0 nm. The surface site density (or) site concentration for the specific surface area (Ns) of rGONF was calculated using potentiometric titration and was found to be 0.00238 $mol \cdot g^{-1}$, which is higher than that for the GO and $NiFe_2O_4$ [19]. Thus, the high surface area with high surface site density of rGONF can have potentially advantageous for the adsorptive removal of pollutants.

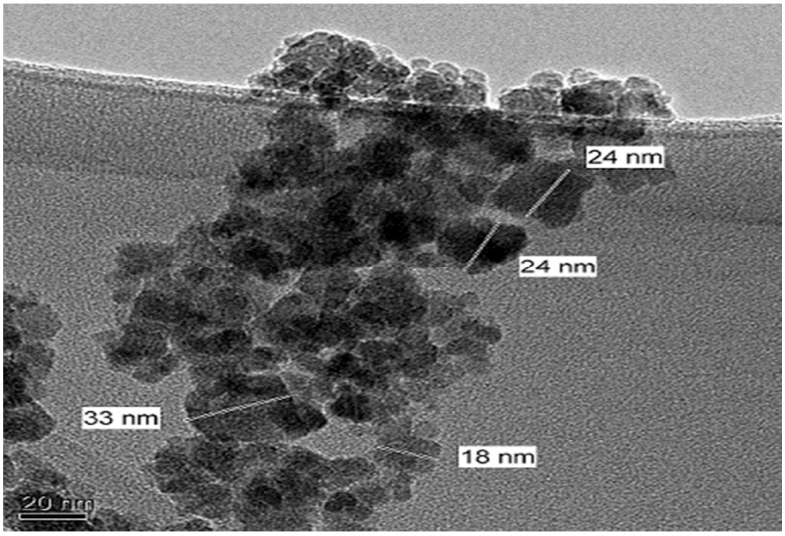

Figure 2. High-Resolution Transmission Electron Microscope image of rGONF (Scale bar is 20 nm).

3.1.3. Magnetic Characterization of Prepared rGONF

Magnetic measurements of rGONF were performed using a SQUID magnetometer (MPMS–7, Quantum Design, San Diego, CA, USA) and the results are shown in Figure 3. Figure 3a indicates the changes of magnetization of rGONF with external magnetic field. However, the obtained magnetic intensity of rGONF (31.6 emu·g^{-1} at 300 K) is lower than that of bulk $NiFe_2O_4$ (60 emu·g^{-1}) due to the presence of rGO and the small size of the $NiFe_2O_4$ nanoparticles in rGONF. Figure 3 b indicates the effect of temperature on the magnetization of rGONF at 100 Oe. The rGONF composites exhibit a superparamagnetic state with small remnant magnetization and coercivity at room temperature which is desirable for many practical applications, so that strong magnetic signals at small applied magnetic fields are obtained. The rGONF composites dispersed in water solution (1 mg·mL^{-1}) can be separated from water by using an external magnet. The separation is almost completed after 10 s with an applied magnetic field of 20 mT.

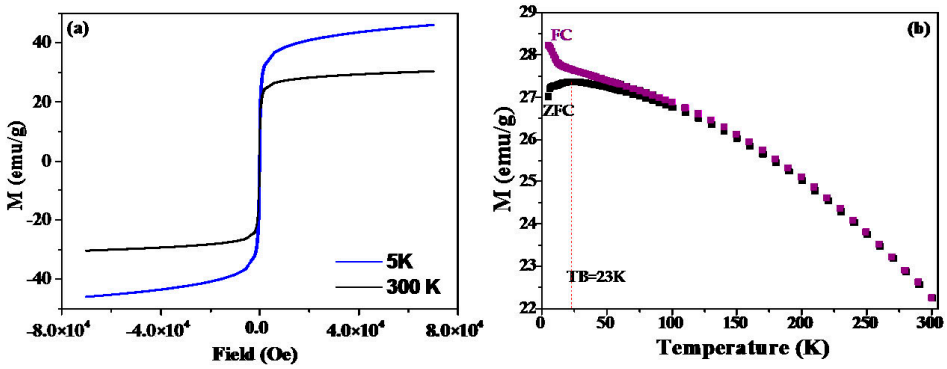

Figure 3. Magnetic measurement of rGONF using a SQUID magnetometer. The trend of magnetization (M) of rGONF with external magnetic field (**a**) and the temperature at 100 Oe (**b**).

3.1.4. Adsorption Mechanism of rGONF for the Removal of Pb(II) and Cr(III)

To understand the adsorption mechanism, the Fourier Transfer-Infrared Resonance (FT-IR) spectrum (Figure 4a) of rGONF loaded with heavy metal ions was studied. Shifting of the absorption peaks of the –C–O, –C–C=C–, and –OH functional groups and Fe–O (520 to 560 cm^{-1}) bond stretching vibration peaks of rGONF to a lower wave number by loading Pb(II) and Cr(III) was observed.

However, the –C–C=C– functional groups and Fe–O of rGONF were effectively shifted more than that of –C–O and –OH. This shifting may be related with the adsorption of Pb(II) and Cr(III) onto rGONF by the chemical interaction between the metal ions and rGONF surface functional groups such as –C–O, –C–C=C–, and –OH, along with oxygen in the Fe–O bond of ferrite. However, the π-electrons of –C–C=C– of graphene oxide along with oxygen in the Fe–O bond of ferrite have a major role for the adsorption of Pb(II) and Cr(III) rather than that of –C–O and –OH functional groups of rGONF. The SEM-surface morphology (Figure 4b) of metal ion loaded rGONF was different compared to that of bare rGONF, supporting the Pb(II) and Cr(III) adsorption onto rGONF. The overall obtained results described the chemical interactions or complexed surface interactions between the homogeneous surface functional groups of rGONF and the metal ions causing chemisorption. A schematic representation of the possible adsorption mechanism has been shown in Figure 5.

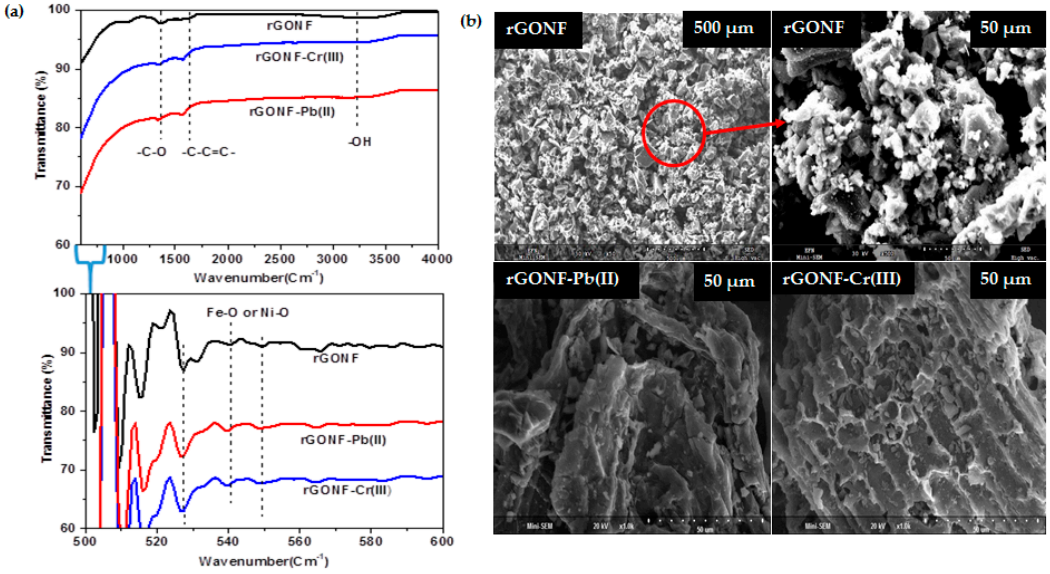

Figure 4. Fourier Transfer-Infrared Resonance (FT-IR) spectra of rGONF (**a**) and scanning electron microscopy images of rGONF and metal ion loaded rGONF (**b**). (The dotted lines indicate the functional groups and its comparative shifting of peaks by loading; the high-resolution of red circled in Figure 4b indicates the highly porous nature of rGONF).

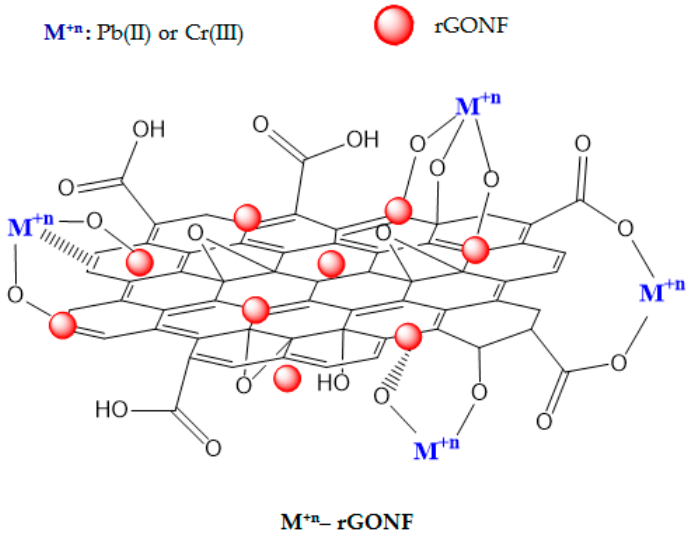

Figure 5. The possible adsorption mechanism of metal ions with rGONF.

3.2. Factors Affecting the Removal of Metal Ions by Using rGONF

3.2.1. Time Profile and Adsorbent Dosage Studies

Figure 6a,b shows that the removal of Pb(II) and Cr(III) with rGONF was rapid and immediately (within 5 min) reached 99% maximum adsorptive removal of Pb(II) and Cr(III). As the contact time further increased to 90 min, the adsorption percentage becomes constant. Therefore, the contact time can be optimized to 30 min for both Pb(II) and Cr(III) with rGONF, respectively.

The effect of the adsorbent dosage (Figure 6c) on the adsorption of Pb(II) and Cr(III) (10 $mg \cdot L^{-1}$) was studied by varying the dosage from 0.1 to 0.8 $g \cdot L^{-1}$ at pH 5 for Pb(II) and pH 4 for Cr(III). The obtained results revealed that the adsorption efficiency and adsorption capacity showed an inverse relationship with the rGONF dose. The maximum adsorption efficiency, 99.7% for Pb(II) and Cr(III), was achieved with 0.4 $g \cdot L^{-1}$ rGONF dosage for Pb(II) and Cr(III), respectively.

3.2.2. pH and Ionic Strength Effect

The effects of solution pH on the adsorption of Pb(II) and Cr(III) onto rGONF were studied by varying the aqueous solution pH (Figure 6d). The adsorption of Pb(II) rapidly increased from pH 2.0 to 3.0, then slowly increased and reached maximum adsorption percentage at pH 4.0 to 5.0 for Pb(II). While the adsorption of Cr(III) was not rapidly increased from pH 2.0 to 3.0, then slowly increased and reached maximum adsorption percentage at pH 4.0 for Cr(III). At lower pH, the high H^+ concentration was competitive with both metal ions that caused low adsorption. As the solution pH increased, the adsorption of metal ions on the rGONF increased due to the decreasing H^+ ion concentration which acted as a competitor to the positive metal ions for adsorption sites on the surface of the nanocomposites. However, the high adsorption of both metal ions onto rGONF at pH < pH of zero-point charge (pHzpc) (6.20) (The pHzpc and acid-base property of nanocomposite was measured by the acid-base titration method as well as the initial and final pH measurement in aqueous solutions (Figure S1). The calculation details were reported at footnote of Figure S1) of rGONF and independent of ionic strength indicates that the adsorption process was not an electrostatic interaction and may be the inner-sphere chemical interaction. The inner-sphere chemical complexation of the adsorption of metal ions was proven from the 2-pKa-diffusion model (illustrated by the Visual Minteq-3.0 program) (Figure 7), where the experimental adsorption data was in close agreement with the model fitting. Above pH 6.0, the surface charges of rGONF became more negative and may cause increased adsorption of metal ions. However, adsorption experiments were not studied above pH 6.0 where the metal ions can precipitate as their hydroxide complexes in aqueous solutions [17]. Therefore, further adsorption studies of both metal ions, Pb(II) and Cr(III), were studied at pH 5.0 and pH 4.0, respectively.

The ionic strength/background ions' effect on the adsorption of both metal ions onto rGONF was studied using NaCl, KCl, and $MgCl_2$ as background electrolytes ranging from 0.0 to 0.5 $mg \cdot L^{-1}$ (Figure S2). From Figure S2, it was clearly observed that there were no significant changes that occurred in the adsorption of Pb(II) (10 $mg \cdot L^{-1}$) and Cr(III) (10 $mg \cdot L^{-1}$) onto rGONF with the increase of the background ions' concentration/ionic strength.

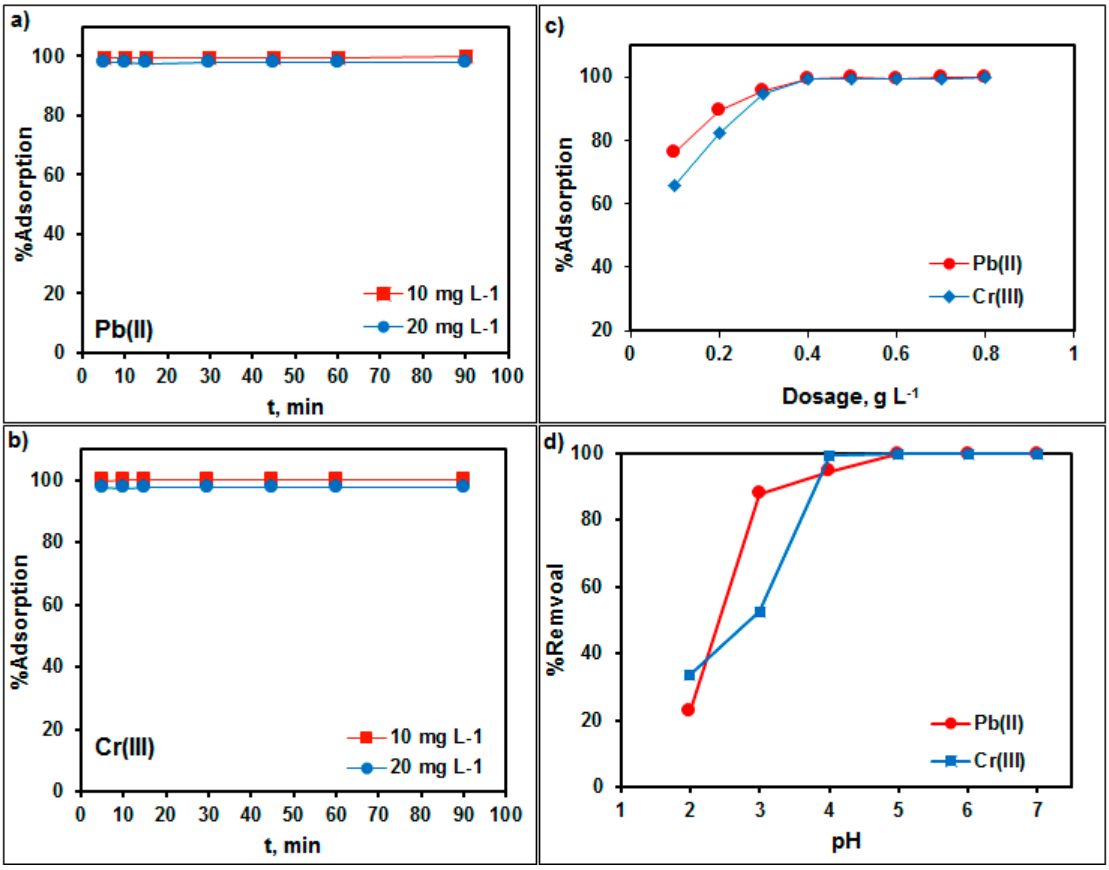

Figure 6. Factors such as equilibrium time (**a**,**b**), rGONF dosage (**c**), and aqueous solution pH (**d**) effect on the adsorption of Pb(II) and Cr(III) onto rGONF at 298 ± 2 K.

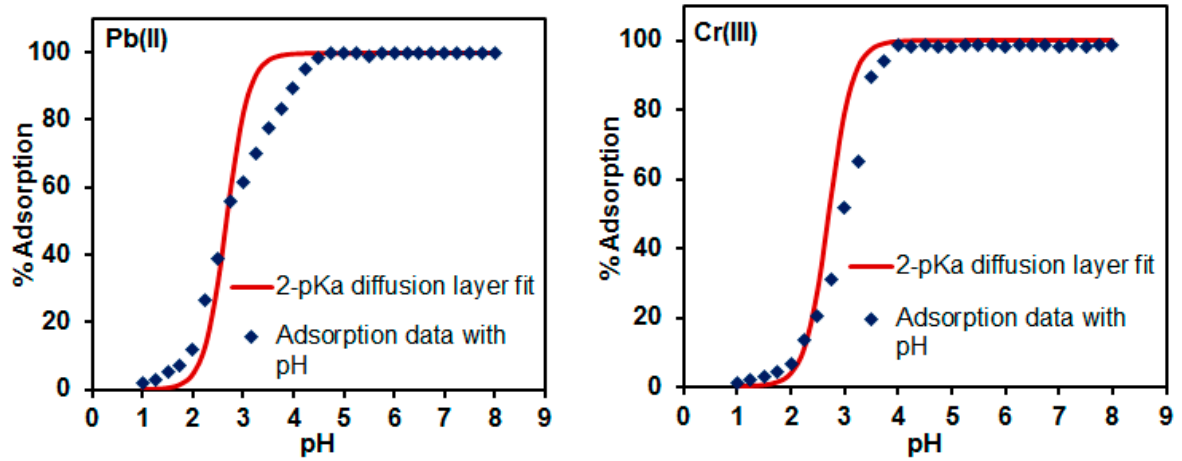

Figure 7. 2-pKa-diffusion layer model fitting of the adsorption data with pH for Pb(II) and Cr(III) onto rGONF.

3.3. Evaluation of Metal Ions Uptake Characteristics of rGONF by the Adsorption Isotherms

After finding the optimum time, dosage, and pH of the metal ions, adsorption isotherm experiments were performed for the evaluation of the metal uptake mechanism and capacity. Various adsorption models such as Langmuir, Freundlich, and Tempkin were used for the experimental isotherms data as shown in Figure 8. The three-isotherm model linear fitting was shown in Figure S3.

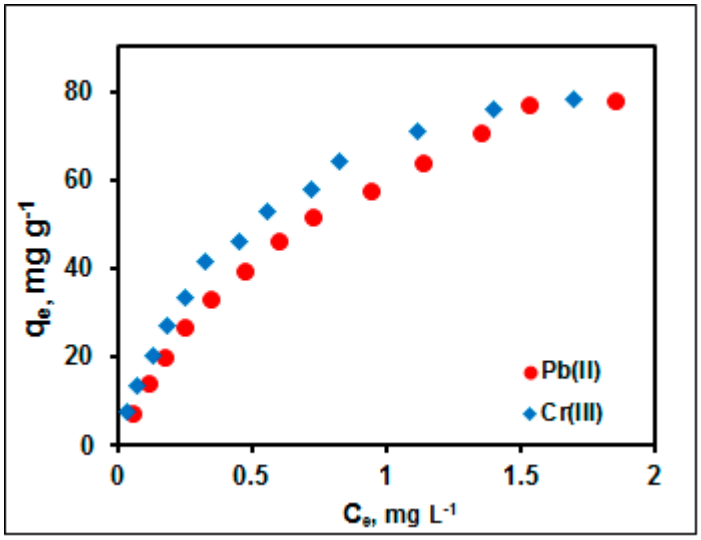

Figure 8. Adsorption isotherms of Pb(II) and Cr(III) (C_o = 2.0 to 25.0 mg·L^{-1}) onto rGONF at pH 5.0 for Pb(II) and pH 4.0 for Cr(III), at 30 min equilibrium time for the range of reaction temperatures, 298–328 ± 2.0 K.

The calculated isotherm parameters, correlation coefficient (R^2) values, and standard deviations in the measurement were used for the evaluation of the suitability of the isotherms and are summarized in Table 3. The Langmuir adsorption isotherm data fit well with the experimental adsorption data compared to the other two models. The adsorption parameters are summarized in Table 3. Hence, the adsorption of Pb(II) and Cr(III) onto rGONF was a monolayer chemisorption on the homogeneous surface. The adsorption capacity of rGONF was greater than that of GO-alone due to the high electron transfer charge of rGONF by $NiFe_2O_4$. The adsorption isotherms and kinetics of GO alone and $NiFe_2O_4$ are shown in Figure S4. The maximum adsorption capacity of rGONF at 298 ± 2 K for Pb(II) and Cr(III) was higher or near to the previously reported values (Table 1), indicating rGONF to be a promising and better adsorbent for heavy metal adsorption. It was also clearly observed from Table 1 that the adsorption capacity of rGONF was higher than the GO and $NiFe_2O_4$ indicates the synergistic enhancement of the adsorption metal ion onto rGONF. The high adsorption of rGONF may be due to the fact that the rGONF has a high surface area and high surface site density when compared with GO and $NiFe_2O_4$ [19]. The distribution of Pb(II) and Cr(III) between the rGONF solution in equilibrium over a range of concentrations at three different temperatures (298–328 K) was studied. From the Langmuir isotherm model, the calculated maximum adsorption capacities (q_{max}) were increased as the temperature increased from 298 to 328 K for both metal ions and the results are shown in Table 4. The increasing adsorption capacity with increasing temperature is associated with endothermic adsorption of metal ions onto rGONF at equilibrium. Hence, the adsorption process was favorable and rapid.

Table 3. Isotherm parameters of Pb(II) and Cr(III) (C_o = 2.0 to 25 mg·L^{-1}) adsorption onto rGONF at 0.4 g·L^{-1} dosage and 298 ± 2 K for 30 min (n = 3, mean ± SD).

Metal Ion	Nano-Composite	Langmuir			Freundlich			Temkin		
		q_{max}, mg·g^{-1}	K_L, L·mg^{-1}	R^2	K_F, mg·g^{-1} (L·mg^{-1})$^{1/n}$	n	R^2	K_T, L·mg^{-1}	B	R^2
Pb(II)	rGONF	121.95 ± 0.20	1.78 ± 0.04	0.991	59.25 ± 0.12	1.42 ± 0.01	0.977	26.40 ± 0.03	52.16 ± 0.25	0.967
	GO	44.56 ± 0.16	0.16 ± 0.16	0.994	8.35 ± 0.18	0.56 ± 0.24	0.893	0.86 ± 0.26	12.46 ± 0.16	0.856
Cr(III)	rGONF	126.58 ± 0.30	1.93 ± 0.04	0.995	57.08 ± 0.21	1.53 ± 0.01	0.974	25.63 ± 0.06	55.74 ± 0.32	0.967
	GO	36.45 ± 0.36	0.86 ± 0.22	0.994	10.46 ± 0.26	0.86 ± 0.35	0.856	2.46 ± 0.12	13.26 ± 0.21	0.921

Table 4. Langmuir isotherm parameters of Pb(II) and Cr(III) (C_o = 2.0 to 25 mg·L^{-1}) adsorption onto rGONF at pH 5.0 for Pb(II) and pH 4.0 for Cr(III), with 30 min equilibrium time for the range of reaction temperatures, 298–328 K (n = 3, mean ± SD).

Metal Ions	q_{max} (mg·g^{-1})		
	298 K	308 K	328 K
Pb(II)	121.95 ± 0.20	130.95 ± 0.20	142.45 ± 0.20
Cr(III)	126.58 ± 0.30	135.55 ± 0.32	148.36 ± 0.24

3.4. Regeneration of Saturated rGONF

The recycling and reuse of the adsorbent is an economic necessity. The metal ions' (Pb(II) and Cr(III)) adsorption capacity was low at low pH, and acid treatment is a more suitable approach for the regeneration of rGONF. 1.0 mol·L^{-1} HNO_3 solution was used for the regeneration of rGONF for both metal ions (initial concentration = 10 ppm) and the desorption efficiency was found to be 92%. The adsorption−desorption cycles were repeated five times using the same batch of rGONF (Figure 9). Comparing the first cycle adsorption with the fifth cycle, the adsorption was decreased to 83%, indicating good regeneration and reusability of rGONF. The slight decrease in the adsorption capacity was attributed to the incomplete desorption of Pb(II) and Cr(III) from the surface of rGONF. Even after five cycles, the magnetic intensity of rGONF was not decreased and the adsorbent could be separated from the solution within 10 s. In addition, the leaching amount of Ni or Fe from the composite into the solution was nearly 0.02 mg·L^{-1}, and the dissolution of the Ni and Fe was under the Environmental Protection Agency (EPA) standard level. The overall results indicate that the prepared magnetic composite can be easily recycled and reused for four cycles, which can be applied in water purification over the long-term. Hence, the synthesized rGONF could be justified as an efficient adsorbent and reasonable for the treatment of heavy metals. In addition, rGONF can be easily separated by an external magnetic field without the loss of any structural changes and can be reused.

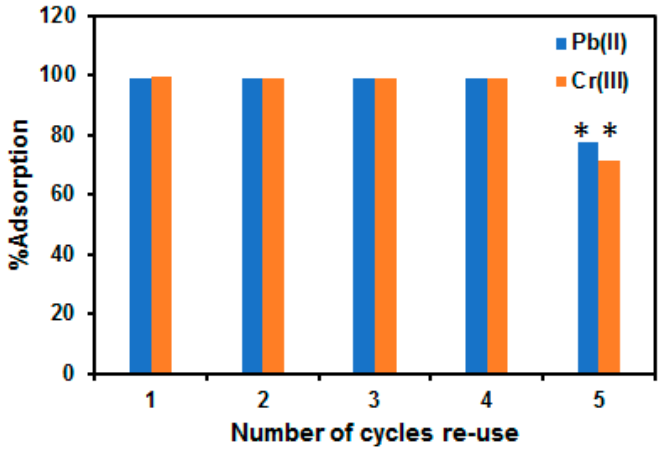

Figure 9. The recycling and reuse studies of the rGONF loaded with Pb(II) and Cr(III). ** indicates significant changes in the adsorption percentage of the metal ions.

3.5. Advantages of the as Prepared rGONF

Based on the overall results, the as prepared rGONF nanocomposite was a good adsorbent and has enhanced adsorptive removal of Pb(II) and Cr(III) as compared to bare GO and $NiFe_2O_4$. The rGONF can easily be recovered from aqueous solutions with an external magnetic field, thus overcoming the problems associated with the filtration, centrifugation, or gravitational separation of the bare adsorbents from aqueous solutions. On the other hand, rGONF can maintain an initial adsorption capacity for up to four cycles, which proved that it is an efficient adsorbent for heavy metal removal.

The adsorption capacity of rGONF for Pb(II) and Cr(III) is comparable and reasonable when compared to the previously reported nanocomposites (Table 1) as well as with GO and $NiFe_2O_4$. Moreover, the adsorption capacity is increased with temperature increases. The preparation cost of rGONF is 100 USD·kg^{-1} (on a small-scale) which is comparable with the often-used nanocomposites. Hence, as prepared rGONF could be justified as an efficient adsorbent and reasonable for the treatment of heavy metals from aqueous effluents.

3.6. Application of the as Prepared rGONF for Pb(II) and Cr(III) Spiked Real Ground Water

In order to see the applicability of the rGONF for the adsorptive removal of both heavy metals from real ground water, water was collected from Yullyang-dong, Sangdang-gu, Cheongju-Si, Republic of Korea. It was spiked with 10 mg·L^{-1} concentration of Pb(II) or Cr(III) and the removal and recycling results are shown in Table 5. Both ions were almost adsorbed from spiked real samples. After the adsorptive removal of both ions, the remaining heavy metal ion concentrations in the real samples reached the EPA permission levels (0.015 to 0.05 mg·L^{-1}) [6]. This result suggests that the nanocomposite used in this work can be successfully applied for the treatment of real ground water containing Pb(II) and Cr(III).

Table 5. Adsorptive removal of Pb(II) and Cr(III) from spiked real ground water collected from Yullyang-dong, Sangdang-gu, Cheongju-Si, Republic of Korea (N = 3, mean values reported here, the standard deviation is less than 2%).

Sample Number	Pb(II) Added, mg·L^{-1}	Cr(III) Added, mg·L^{-1}	Adsorption Amount, mg·g^{-1}	
			Pb(II)	Cr(III)
1	4.0	4.0	3.963	3.965
2	6.0	6.0	5.980	5.989
3	10.0	10.0	9.983	9.972

We also conducted batch adsorption and desorption experiments for the spiked real ground water sample with the developed procedure for the evaluation of the real field applicability or real field re-usability of the adsorbent and the obtained results are shown in Figure 10. The obtained results showed that the developed method can be re-used up to four cycles with more than 99% adsorption of both metal ions. However, the desorption capacity decreased with increasing the re-use cycles.

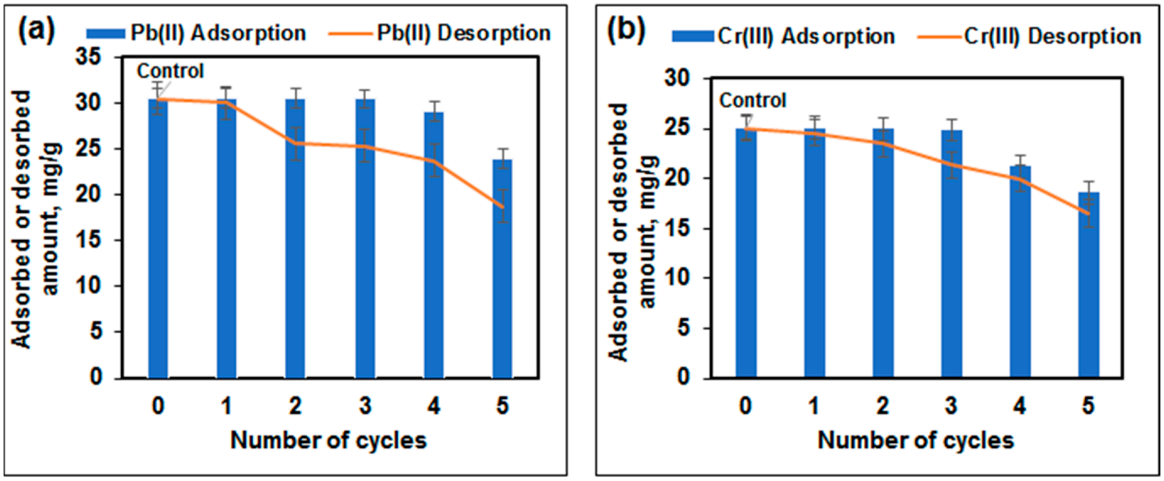

Figure 10. Adsorption and desorption studies of metal ion spiked real ground water samples by using rGONF (0.4 g·L^{-1}) for Pb(II) (12.19 mg·L^{-1}) (**a**) and Cr(III) (10.03 mg·L^{-1}) (**b**) at room temperature.

4. Conclusions

Reduced Graphene Oxide Nickel Ferrite (rGONF) was successfully prepared by the co-precipitation method. The prepared rGONF was confirmed by Raman, XPS, and FT-IR spectral studies. The TEM and BET surface characterization results determined the nanosize of rGONF (34.46 nm) with a high surface area of 167.26 $m^2 \cdot g^{-1}$, which is higher than that of GO and $NiFe_2O_4$. The potentiometric titrations confirmed that the surface site density is around 0.0028 $mol \cdot g^{-1}$, which is higher than the bare rGONF. The magnetic measurements confirmed that rGONF had a superparamagnetic nature and was easily collected by an external magnetic field in a few seconds, achieving a fast and efficient removal of heavy metals (Pb(II) and Cr(III)) from water. The adsorption isotherm results confirmed that the adsorption of Pb(II) and Cr(III) was a monolayer adsorption on the homogenous surface of the nanocomposite, rGONF. The adsorption capacity of Pb(II) and Cr(III) increases with increasing temperature. In the present investigations, the adsorptive removal of the metal ions was achieved under the EPA permissible levels. In addition, for both metal ions, the adsorption capacity of rGONF was enhanced with the rapid adsorption process than that of the bare rGONF.

The overall results conclude that the chemical interactions or complexed surface interactions between the homogeneous surface functional groups of rGONF and the metal ions cause chemisorption. Hence, the synthesized rGONF could be justified as an efficient adsorbent and reasonable for the treatment of heavy metals. In addition, rGONF can be easily separated by an external magnetic field without the loss of any structural changes and can be reused up to four cycles. The field applicability of the developed method was tested with metal ion spiked real ground water samples and the results showed that rGONF can be re-used up to four cycles with more than 99% adsorption of both metal ions. During the first cycle, the removal of Pb(II) and Cr(III) reached the EPA permissible level. However, the desorption capacity of the adsorbed metal ions deceased with an increasing number of re-use cycles. The present rGONF nanocomposite cannot be used directly in continuous column experiments due to the small particle size, and the nanocomposite has to be developed further to be applied in real water systems, where batch treatment is not suitable.

Supplementary Materials: The following supplementary materials available for review: http://www.mdpi.com/2075-4701/7/6/225/s1. Figure S1: Acid base properties of rGONF in aqueous suspension. pH changes with rGONF alone in aqueous solutions (**a**,**b**). The acid-base titration curves of rGONF with 0.1 $mol \cdot L^{-1}$ HNO_3 (**c**) and 0.1 $mol \cdot L^{-1}$ NaOH (**d**) for measuring pKa_1 and pKa_2 to calculate pHzpc of rGONF. (Note: pH_i: initial pH; pH_f: final pH, ΔpH: difference in pH_f and pH_i; $[H^+]$: H^+ concentration; Q = Coulomb charge density). The pKa_1 and pKa_2 were measured from the intercepts of the curves (**c**,**d**), respectively. Where Ka_1 = 1/Intercept of curve (**c**), Ka_2 = Intercept of curve (**d**). Hence, $pKa_1 = -Log(1/Intercept)$; $pKa_2 = -Log(Intercept)$, Figure S2: Ionic strength effect on adsorption removal of Pb(II) and Cr(III) by using rGONF at pH 5.0 for Pb(II) (10 $mg \cdot L^{-1}$) and pH 4.0 for Cr(III) (10 $mg \cdot L^{-1}$), and 30 min equilibrium time for the range of reaction temperature, 298–328 ± 2.0 K, Figure S3: Linear fitting of adsorption isotherm models to the adsorptive isotherm data of Pb(II) and Cr(III) (C_o = 2.0 to 25 mg L^{-1}) onto rGONF at pH 5.0 for Pb(II) and pH 4.0 for Cr(III), and 30 min equilibrium time for the range of reaction temperature, 298–328 ± 2.0 K. Figure S4: Adsorptive kinetics (**a**,**b**) and isotherms (**c**,**d**) of Pb(II) and Cr(III) (C_o = 2.0 to 25 mg L^{-1}) onto GO and NiF_2O_4 at pH 5.0 for Pb(II) and pH 4.0 for Cr(III), and 30 min equilibrium time for the range of reaction temperature, 298–328 ± 2.0 K.

Acknowledgments: This work was supported by a Research grant–2017 from Kwangwoon University, Seoul, Korea and was partly supported by the Korean Ministry of Environment as the "GAIA project (2014000550003)".

Author Contributions: Lakshmi Prasanna Lingamdinne, Janardhan Reddy Koduru, and Yoon-Young Chang conceived and designed the experiments; Lakshmi Prasanna Lingamdinne and Im-Soon Kim performed the experiments; Jeong-Hyub Ha contributed analysis tools; Janardhan Reddy Koduru and Jae-Kyu Yang analyzed the data and wrote the paper.

Conflicts of Interest: The authors declare no conflict of interest.

References

1. Dreyer, D.R.; Park, S.; Bielawski, C.W.; Ruoff, R.S. The chemistry of graphene oxide. *Chem. Soc. Rev.* **2010**, *39*, 228–240. [CrossRef] [PubMed]
2. Chung, C.; Kim, Y.K.; Shin, D.; Ryoo, S.R.; Hong, B.H.; Min, D.H. Biomedical applications of graphene and graphene oxide. *Acc. Chem. Res.* **2013**, *46*, 2211–2224. [CrossRef] [PubMed]
3. Kyzas, G.Z.; Deliyanni, E.A.; Matis, K.A. Graphene oxide and its application as an adsorbent for wastewater treatment. *J. Chem. Technol. Biotechnol.* **2014**, *89*, 196–205. [CrossRef]
4. Zhu, J.; Wei, S.; Gu, H.; Rapole, S.B.; Wang, Q.; Luo, Z.; Haldolaarachchige, N.; Young, D.P.; Guo, Z. One-pot synthesis of magnetic graphene nanocomposites decorated with core@ double-shell nanoparticles for fast chromium removal. *Environ. Sci. Technol.* **2011**, *46*, 977–985. [CrossRef] [PubMed]
5. Zhu, J.; Chen, M.; Qu, H.; Zhang, X.; Wei, H.; Luo, Z.; Colorado, H.A.; Wei, S.; Guo, Z. Interfacial polymerized polyaniline/graphite oxide nanocomposites toward electrochemical energy storage. *Polymer* **2012**, *53*, 5953–5964. [CrossRef]
6. Fan, L.; Luo, C.; Sun, M.; Qiu, H. Synthesis of graphene oxide decorated with magnetic cyclodextrin for fast chromium removal. *J. Mater. Chem.* **2012**, *22*, 24577–24583. [CrossRef]
7. Li, J.; Zhang, S.; Chen, C.; Zhao, G.; Yang, X.; Li, J.; Wang, X. Removal of Cu(II) and fluvic acid by graphene oxide nanosheets decorated with Fe_3O_4 nanoparticles. *ACS Appl. Mater. Interfaces* **2012**, *4*, 4991–5000. [CrossRef] [PubMed]
8. Hu, X.; Liu, Y.; Wang, H.; Chen, A.; Zeng, G.; Liu, S.; Guo, Y.; Hu, X.; Li, T.; Wang, Y.; et al. Removal of Cu(II) ions from aqueous solution using sulfonated magnetic graphene oxide composite. *Sep. Purif. Technol.* **2013**, *108*, 189–195. [CrossRef]
9. Gollavelli, G.; Chang, C.C.; Ling, Y.C. Facile Synthesis of smart magnetic graphene for safe drinking water: Heavy metal removal and disinfection control. *ACS Sustain. Chem. Eng.* **2013**, *1*, 462–472. [CrossRef]
10. Lingamdinne, L.P.; Choi, Y.L.; Kim, I.S.; Chang, Y.Y.; Koduru, J.R.; Yang, J.K. Porous graphene oxide based inverse spinel nickel ferrite nanocomposites for the enhanced adsorption removal of arsenic. *RSC Adv.* **2016**, *6*, 73776–73789. [CrossRef]
11. Yao, Y.; Miao, S.; Liu, S.; Ma, L.P.; Sun, H.; Wang, S. Synthesis, characterization, and adsorption properties of magnetic Fe_3O_4@graphene nanocomposite. *Chem. Eng. J.* **2012**, *184*, 326–332. [CrossRef]
12. Deng, J.H.; Zhang, X.R.; Zeng, G.M.; Gong, J.L.; Niu, Q.Y.; Liang, J. Simultaneous removal of Cd(II) and ionic dyes from aqueous solution using magnetic graphene oxide nanocomposite as an adsorbent. *Chem. Eng. J.* **2013**, *226*, 189–200. [CrossRef]
13. Zhang, W.; Shi, X.; Zhang, Y.; Gu, W.; Li, B.; Xian, Y. Synthesis of water-soluble magnetic graphene nanocomposites for recyclable removal of heavy metal ions. *J. Mater. Chem. A* **2013**, *1*, 1745–1753. [CrossRef]
14. Sun, H.; Cao, L.; Lu, L. Magnetite/reduced graphene oxide nanocomposites: One step solvothermal synthesis and use as a novel platform for removal of dye pollutants. *Nano Res.* **2011**, *4*, 550–562. [CrossRef]
15. Ai, L.; Zhang, C.; Chen, Z. Removal of methylene blue from aqueous solution by a solvothermal-synthesized graphene/magnetite composite. *J. Hazard. Mater.* **2011**, *192*, 1515–1524. [CrossRef] [PubMed]
16. Bai, S.; Shen, X.; Zhong, X.; Liu, Y.; Zhu, G.; Xu, X.; Chen, K. One-pot solvothermal preparation of magnetic reduced graphene oxide-ferrite hybrids for organic dye removal. *Carbon* **2012**, *50*, 2337–2346. [CrossRef]
17. Lingamdinne, L.P.; Koduru, J.R.; Choi, Y.L.; Chang, Y.Y.; Yang, J.K. Studies on removal of Pb(II) and Cr(III) using graphene oxide based inverse spinel nickel ferrite nanocomposite as sorbent. *Hydrometallurgy* **2016**, *165*, 64–72. [CrossRef]
18. Maaz, K.; Karim, S.; Mumtaz, A.; Hasanain, S. K.; Liu, J.; Duan, J.L. Synthesis and magnetic characterization of nickel ferrite nano particles prepared by co-precipitation route. *J. Magn. Magn. Mater.* **2009**, *321*, 1838–1842. [CrossRef]
19. Lingamdinne, L.P.; Choi, Y.L.; Kim, I.S.; Yang, J.K.; Koduru, J.R.; Chang, Y.Y. Preparation and characterization of porous reduced graphene oxidebased inverse spinel nickel ferrite nanocomposite for adsorption removal of radionuclides. *J. Hazard. Mater.* **2017**, *326*, 145–156. [CrossRef] [PubMed]
20. Zhang, Y.; Tang, Z.R.; Fu, X.; Xu, Y.J. TiO_2–graphene nanocomposites for gas-phase photocatalytic degradation of volatile aromatic pollutant: Is TiO_2–graphene truly different from other TiO_2–carbon composite materials? *ACS Nano* **2010**, *4*, 7303–7314. [CrossRef] [PubMed]

21. Abu-Zurayk, R.A.; Bakain, R.Z.A.; Hamadneh, I.; Al-Dujaili, A.H. Adsorption of Pb(II), Cr(III) and Cr(VI) from aqueous solution by surfactant-modified diatomaceous earth: Equilibrium, kinetic and thermodynamic modeling studies. *Int. J. Miner. Process.* **2015**, *140*, 79–87. [CrossRef]
22. Yang, S.; Li, L.; Pei, Z.; Li, C.; Lv, J.; Xie, J.; Wen, B.; Zhang, S. Adsorption kinetics, isotherms and thermodynamics of Cr(III) on graphene oxide. *Colloids Surf. A Physicochem. Eng. Asp.* **2014**, *457*, 100–106. [CrossRef]
23. Lingamdinne, L.P.; Koduru, J.R.; Jyothi, R.K.; Chang, Y.Y.; Yang, J.K. Factors effect on bioremediation of Co(II) and Pb(II) onto *Lonicera japonica* flowers powder. *Desalin. Water Treat.* **2016**, *57*, 13066–13080. [CrossRef]
24. Reddy, D.H.K.; Lee, S.M. Three-dimensional porous spinel ferrite as an adsorbent for Pb(II) removal from aqueous solutions. *Ind. Eng. Chem. Res.* **2013**, *52*, 15789–15800. [CrossRef]
25. Ahmet, S.; Mustafa, T.; Mustafa, S. Adsorption of Pb(II) and Cr(III) from aqueous solution on Celtek clay. *J. Hazard. Mater.* **2007**, *144*, 41–46.